

Article

Coupled Excitation Strategy for Crack Initiation at the Adhesive Interface of Large-Sized Ultra-Thin Chips

Tao Wu ^{*} , Xin Chen, Shiju Wen, Fangsong Liu and Shengping Li

College of Engineering, Shantou University, Shantou 515063, China; 21xchen@stu.edu.cn (X.C.); 22sjwen@stu.edu.cn (S.W.); 22fslu@stu.edu.cn (F.L.); spli@stu.edu.cn (S.L.)

* Correspondence: taowu@stu.edu.cn

Abstract: The initial excitation of interface crack of large-size ultra-thin chips is one of the most complicated technical challenges. To address this issue, the reversible fracture characteristics of a silicon-based chip (chip size: 1.025 mm × 0.4 mm × 0.15 mm) adhesive layer interface was examined by scanning electron microscope (SEM) tests, and the characteristics of a cohesive zone model (CZM) unit were obtained through peel testing. The fitting curve of the elastic bilinear model was in high agreement with the experimental data, with a correlation coefficient of 0.98. The maximum energy release rate required for stripping was $G_C = 10.3567$ N/m. Subsequently, a cohesive mechanical model of large-size ultra-thin chip peeling was established, and the mechanical characteristics of crack initial excitation were analyzed. The findings revealed that the larger deflection peeling angle in the peeling process resulted in a smaller peeling force and energy release rate (ERR), which made the initial crack formation difficult. To mitigate this, a coupling control method of structure and force surface was proposed. In this method, through structural coupling, the change in chip deflection was greatly reduced through the surface coupling force, and the peeling angle was greatly improved. It changed the local stiffness of the laminated structure, made the action point of fracture force migrate from the center of the chip to near the edge of the chip, the peeling angle was increased, and the energy release rate was locally improved. Finally, combined with mechanical analysis and numerical simulation of the peeling process, the mechanical characteristics of peeling were analyzed in detail. The results indicated that during the initial crack germination process, the ERR of the peel interface is significantly increased, the maximum stress value borne by the chip is significantly reduced, and the peel safety and reliability are greatly improved.

Keywords: cohesion zone model; peeling angle; non-destructive chip peeling of large-size ultra-thin chip; coupling excitation of crack initiation



Citation: Wu, T.; Chen, X.; Wen, S.; Liu, F.; Li, S. Coupled Excitation Strategy for Crack Initiation at the Adhesive Interface of Large-Sized Ultra-Thin Chips. *Processes* **2023**, *11*, 1637. <https://doi.org/10.3390/pr11061637>

Academic Editor:
Raul D. S. G. Campilho

Received: 25 April 2023
Revised: 19 May 2023
Accepted: 22 May 2023
Published: 26 May 2023



Copyright: © 2023 by the authors. Licensee MDPI, Basel, Switzerland. This article is an open access article distributed under the terms and conditions of the Creative Commons Attribution (CC BY) license (<https://creativecommons.org/licenses/by/4.0/>).

1. Introduction

A chip is an integrated circuit manufactured on the surface of a semiconductor chip, which plays an important role in physics, military applications, science and technology, the chemical industry, medicine, and other fields [1–4]. Chip peeling and transfer are widely used for the packaging and manufacturing of high-performance devices, such as CPU, DSP, LED, RFID, and MEMERY, and represent the key to enhancing the performance and reliability of electronic devices. At present, chips are constantly developing in the direction of thinness, high performance, and low power consumption [5–7]. The industry IC chip thickness has been reduced from 120 μm to less than 40 μm , and those used in laboratory applications have reached the level of 10–20 μm . The chip transfer adopts a chip-based film laminate structure, which is characterized by a 5–10 μm adhesive layer between the chip and the base film (made of polyvinyl chloride) [8]. Chip peeling the separation of the interface to realize the separation of the chip and the substrate. As the chip size becomes larger and the thickness becomes thinner, the chip is easily bent and deformed together with the base film during the peeling process, resulting in chip damage or fracture. This problem

is common in the field of high-end electronic packaging and testing equipment, and it is a technical bottleneck restricting the development of related processes, which has resulted in extensive research. Delamination is also a common problem in many other domains such as the aerospace industry when dealing with strain measurement instrumentation or composite delamination, even in rotating parts [9].

The combination of mechanical analysis, finite element simulation, and experimental analysis is a common method to analyze similar problems. Using finite element analysis and building a cohesive zone model, Zou et al. clarified the technical feasibility of an artificial barrier to control crack height [10]. Neves and Khan et al. used the finite element method and the cohesive zone model to study the adhesive joint. The simulation proved to have a good correlation with the experimental results, making it possible to model and design a hybrid model of the adhesive joint [11,12]. Hong et al. proposed the substrate dynamic release layer (DRL) chip structure and established the finite element and bond zone model (CZM) to study the evolution of ultra-thin chip peeling. The results of the model showed that a longer laser irradiation time can produce larger maximum vapor pressure and chip transfer speed [13]. Hong et al. also put forward a spring-buffered chip stripping technology, which can ensure chip stripping and inhibit chip cracking under large ejector pin force [14]. Using linear fracture theory, Yin, Peng, and Liu established the fracture mechanical model of interfacial peeling under impact load and calculated the stress intensity factor at the crack tip, the energy release rate during expansion, and the influencing factors [15,16]. The inaccuracy of the linear analysis in the situation, and the dual-standard competitive failure criterion of chip fragmentation and bending damage, as well as the flexible needle, multi-needle scheme, vacuum, and flexible suction control strategies were proposed. Cheng of Northwestern University in the United States analyzed the transfer process of stamp/ink-type chips, revealing the phenomenon of an initial fracture value at low speeds [17]. Jeon proposed a blowing peeling scheme, where the chip is peeled off by combining an air blowing force under the substrate (≤ 90 kpa) and the appropriate speed of the upper suction nozzle (≤ 50 mm/min) [18]. Behler implemented a step-difference needle to realize peeling of large-size ultra-thin memory chips through the coupling of structure and rate [7]. It can be found that, generally, the simplified beam model and the macroscopic fracture mechanics linear small deformation theory are used to analyze the peeling process. As the size of the chip becomes larger, the thickness becomes thinner, the flexibility of the chip increases, and the deflection during the peeling process becomes larger; the linear small deformation theory still cannot correctly analyze this process, and thus a new mechanical model is needed.

The SEM test in the next section shows that the chip peeling process is essentially the crack tip extension process between the chip and the adhesive layer interface, which can be analyzed by the adhesive interface separation mechanical model. Williams studied the stress and pre-strain in the process of interfacial fracture and proposed a general criterion of initial peeling from the perspective of energy [19]. Molinari focused on the introduction of the cohesive zone model (CZM) in the crack tip region and identified that the size of the cohesion zone is related to the peeling angle [20,21]. Kovalchick and Yang explained that the ERR and peeling rate showed a power-law relationship [22]. Other relevant studies focused on the peeling under rigid substrates, which lay a theoretical foundation for the research of peeling excitation under large deflection and large deformation of flexible substrates [23,24].

This paper is a new attempt to apply the adhesive peel model and CZM unit to chip peeling analysis. In this paper, an adhesive peeling model was established to analyze the initial peeling process. Combined with simulations under a large deformation, the impact of changes in the peeling angle on initial peeling was revealed. On this basis, structural coupling and force surface coupling strategies were proposed, dividing the chip peeling process into two stages; the initial peeling stage and the crack propagation stage, to effectively improve the peeling speed and reduce the stress-strain state of chips.

In this paper, our research is organized as follows:

Section 1 of the research discusses the importance of chip delamination and the proposed approach for analyzing the process. It focuses on the use of adhesive delamination models and CZM elements, along with structural and force-coupling strategies to divide the chip removal process into initial detachment and crack expansion stages.

Section 2 establishes a cohesive fracture mechanics model and analyzes the cohesive force unit model, determining that a bilinear-CZM model is appropriate for describing chip detachment behavior. Furthermore, a mechanical analysis of chip bonding and delamination is conducted to establish the relationship between lifting rate and the energy required for delamination.

Section 3 details the simulation experiments based on the findings from Section 2 and discusses the effects of factors such as chip size and lifting speed on crack initiation and stress during chip removal.

Section 4 proposes a coupling fracture initiation model for adhesive interface cracks, with a focus on the mechanical characteristics of this model.

In Section 5, we simulate the characteristics of crack initiation in large-sized ultra-thin chips and discuss how the delamination angle condition can be improved during crack initiation to reduce the local stress of chip removal.

Finally, Section 6 provides conclusions and outlines plans for further research.

2. Mechanical Modeling and Fracture Analysis of Chip Adhesion Interface

2.1. Adhesion and Peeling Model

The traditional research on chip peeling mainly focuses on the chip–adhesive–substrate structure, using linear small deformation theory and macroscopic fracture mechanics methods to analyze the adhesive layer fracture [25–28].

When the chip size is small and the thickness is large, and the chip deformation can be almost negligible, this model is somewhat representative and can reflect the fracture problem at the interface to a certain extent. As the chip size increases and the thickness decreases, the flexibility of the chip increases, and large deflection deformation occurs during the peeling process. To understand the essential characteristics of adhesive fracture, SEM experiments were conducted. Figure 1 shows the results after multiple round of adhesion and peeling. In Figure 1a, the surface of the epitaxial sheet was smooth with almost no adhesive residue, and the entire peeling process was reversible. On the other hand, Figure 1b presents a clear filament phenomenon at the crack tip region, which undergoes initiation, propagation, and detachment, and the crack tip region presented a common extension distribution.

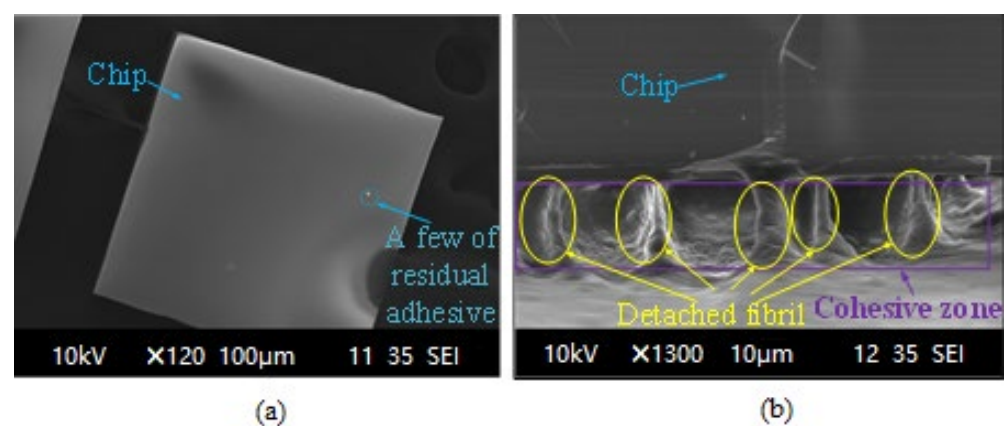


Figure 1. Electron microscope scanning test. (a) Chip epitaxy after multiple peeling; (b) interface separation crack tip.

The results show that the chip peeling process is consistent with the extension process of the crack tip between the chip bonding layer interface, which can be simulated using the CZM model. In reality, the chip peeling is shown in Figure 2, where the central hole on the

upper surface of the needle cover is vacuum-absorbed to fix the chip, and the outer ring hole is vacuum-absorbed to fix the blue film around the chip. During peeling, the chip is pushed up by the needle, and the membrane deformation produces a peel force. Once the peeling force at the junction of the chip and the adhesive layer exceeds the adhesive force, the initial fracture begins to occur.

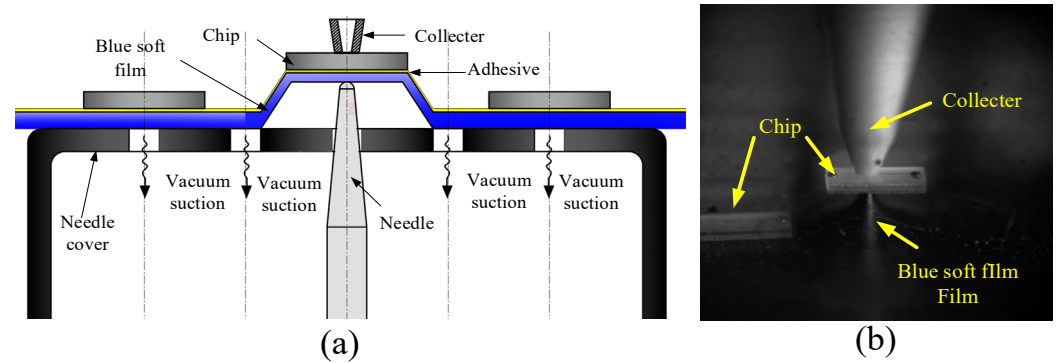


Figure 2. Traditional chip peeling method. (a) Actual peeling process; (b) schematic diagram.

The edge of the suction hole closest to the chip is regarded as the chip peeling fixed support boundary for chip peeling, and the peeling model is illustrated in Figure 3a. During peeling, the chip exhibits symmetrical deformation with the needle tip serving as the fulcrum, as shown in the simplified model depicted in Figure 3b.

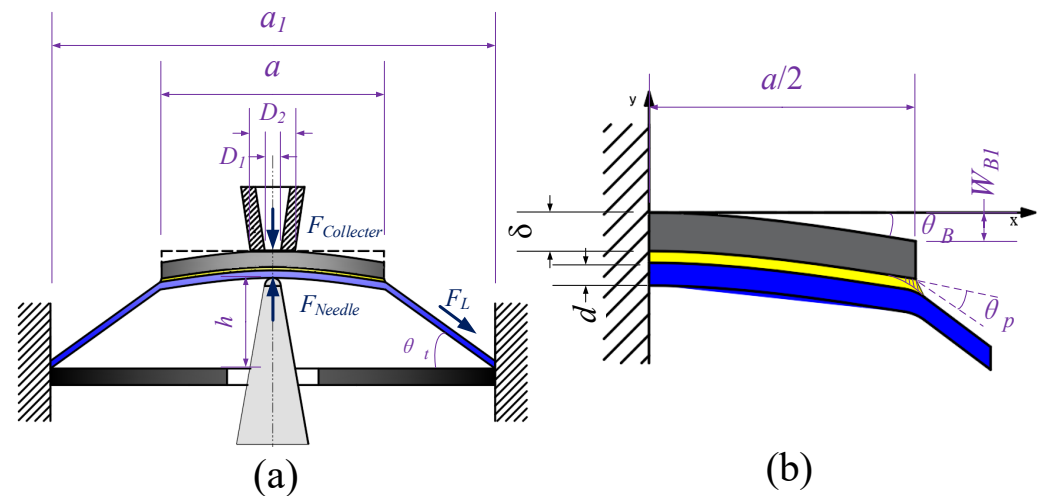


Figure 3. Chip Interface Crack Germination Model. (a) Simplified model; (b) cantilever model.

The figure illustrates various parameters and variables: a_1 is the length of the fixed support boundary, a is the chip length, D_1 is the inner diameter of the contact surface between the needle and the chip, δ is the thickness of the chip, D_2 is the outer diameter of the contact surface between the needle and the chip, d is the thickness of the blue film, and W_{B1} is the largest chip vertical deflection, θ_t is the deflection angle of the soft film, θ_B is the maximum turning angle of the chip, θ_P is the peeling angle, h is the lifting height of the chip, F_{needle} is the force exerted by the ejector pin, $F_{collector}$ represents the downward pressure applied by the collector, and F_L is the blue film pulling force.

2.2. Test for CZM UNIT

Adhesion and peeling are realized through the initiation and extension of the crack tip area. In order to describe the adhesive characteristics more accurately, a CZM cohesion unit was established through experimental measurements to determine the relationship

between deformation and peeling force. Considering that the crack during initiation is mainly an opening mode crack, the probe test method was adopted in the test [29].

The instrument used in the test is the multifunctional push–pull force meter shown in Figure 4. The column is attached to an XY micro-movement translation stage (resolution: 0.002 mm). The Z-direction platform module (resolution: 0.001 mm, effective stroke 75 mm) is integrated with a load cell (accuracy: 0.001 g) at the end. The device samples through sensors and observes the experimental process using a microscope. The comprehensive accuracy error of this platform is within 0.01%, with a minimum speed of 0.01 mm/s and an average resolution of 2 nm.

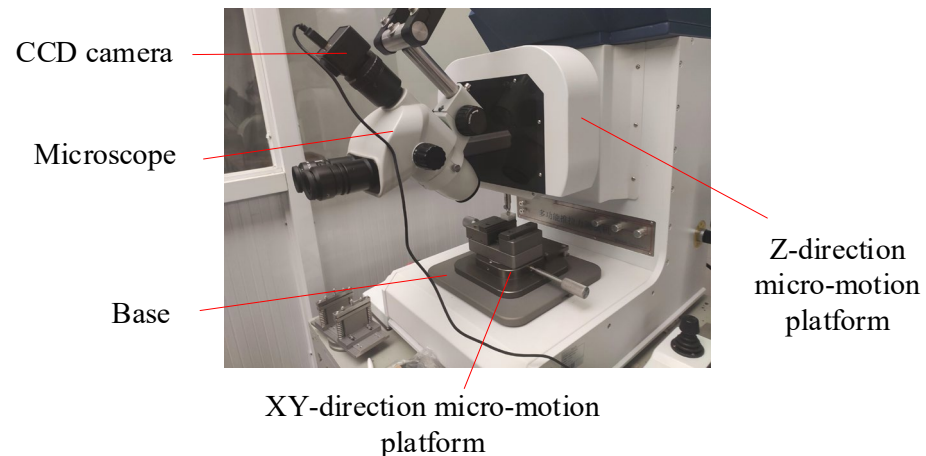


Figure 4. Test instruments.

The experiment was set up as shown in Figure 5. First, clean the glass plate with distilled water, wipe it with an acetone solution and keep it dry until use. Next, cut off part of the blue film (surface protective film, spv-224srb, Nitto, Osaka, Japan) and use ethyl cyanoacrylate to dry it quickly. The adhesive adheres the adhesive surface of the blue film to the substrate. After standing for 3 h, clamp the glass plate on the micro-motion platform of the push–pull tester. Finally, fix the single-sided polished silicon wafer (nanoscale, thickness $650 \pm 20 \mu\text{m}$, crystalline phase P<100>, growth method CZ, resistivity 0–20 Ωcm) on the push–pull knife that pushes the Z-axis. The test steps are as follows:

- (1) Move the Z-axis downward at a constant speed of 0.05 mm/s until the square piece on the broach contacts the blue film and maintain the contact pressure at 10 N;
- (2) Set the holding time to 120 s;
- (3) Control the Z axis to lift at a speed of 1 mm/s;
- (4) Repeat the above steps cyclically to obtain multiple sets of test data.

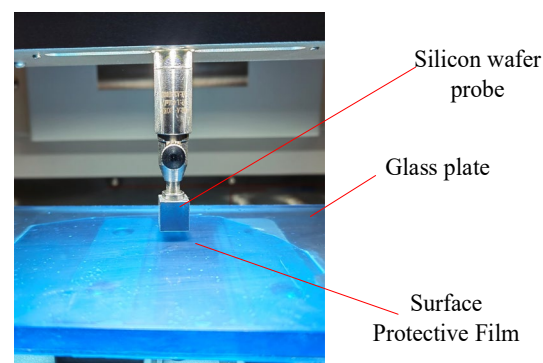


Figure 5. Test specimen and process.

The experiments were conducted at a test environment temperature of 21.2 °C, and the Levenberg–Marquardt iterative algorithm was utilized to fit the stress–displacement curve data acquired during the separation of the blue film from the polished silicon wafer. The fitting curves of the three CZMs are shown in Figure 6. The results show that the fitting curve of the elastic bilinear model (Bilinear–CZM) had the highest agreement with the experimental data, and the correlation coefficient was as high as 0.98. Therefore, the bilinear model (Bilinear–CZM) can be used to describe the chip peeling process. The cohesion model parameters obtained are provided in Table 1.

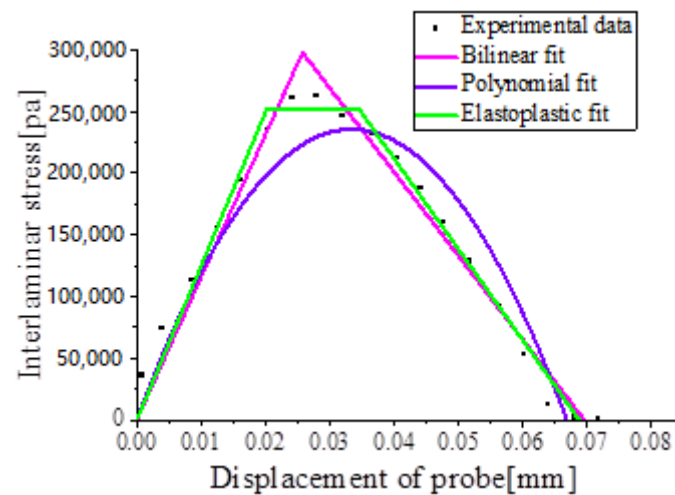


Figure 6. Fitting curves of CZM and experimental data.

Table 1. Fitting parameters of CZM.

CZM Model	σ_{\max}/Pa	δ_0/mm	δ_1/mm	δ_2/mm	$\delta c/\text{mm}$	R^2
Bilinear	297,821.664	0.02576			0.06955	0.97783
Polynomial	235,543.553	0.03341			0.06683	0.88844
Elastoplastic	251,316.990		0.02014	0.03464	0.06877	0.97076

2.3. Mechanical Criterion of Crack Initiation at Adhesive Interface

The mechanical model of chip peeling is similar to Kendall's soft tape peeling model [30,31], as presented in Figure 7. The experimental model uses rigid substrate soft film peeling mechanics. Among them, P_f is the peeling force, θ_0 is the peeling angle, Δc is the length of the cohesive zone, d is the thickness of the soft film, G_c is the unit surface peeling energy, and E_{film} is the elastic modulus of the soft film, E_{chip} is the elastic modulus of the chip. Assuming that the surface bonding energy of the bonding interface per unit area is U_S , when the peeling rate is constant, the adhesive layer absorbs the energy generated by the peeling force W_p and converts it into the cohesive energy of the adhesive layer in the CZM cohesive zone ΔII . As the interface separates, the solid–solid interface between the chip and the adhesive layer is transformed into the solid–gas interface between the chip air and the colloid air, and energy is accumulated within the adhesive layer ΔII . Overcoming the surface energy of bonding interfaces in ΔII , the effective work performed by ΔU_S is called the unit energy release rate G , and the dissipated energy is converted into internal energy, thermal energy, and other energies of the material.

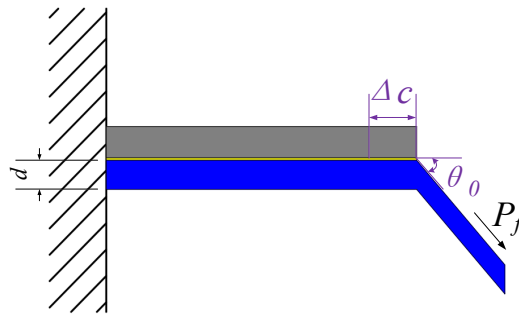


Figure 7. Rigid substrate–soft film peeling mechanical test model.

The relationship between the peeling energy release rate, peeling force, and peeling angle is:

$$G = \frac{P_f^2}{2E_{film}b^2d} + \frac{P_f}{b}(1 - \cos \theta_0) \quad (1)$$

In Equation (1), the first term on the right side of the equation is the deformation energy of the soft film, and the second term is the work done by the peeling force. Assuming that the unit surface peeling energy is G_c , the criterion for crack initiation by interfacial peeling is:

$$G = G_c \quad (2)$$

With a constant G_c , there is a negative correlation between the peeling angle θ_0 and the peeling force P_f . Essentially, as the peeling angle θ_0 decreases, the peeling force P_f increases, and as the peeling angle θ_0 increases, the peeling force P_f reduces. In addition, there is a positive correlation between the energy release rate G and the peeling angle θ_0 , meaning that as the peeling angle θ_0 decreases, the G also decreases and as the peeling angle θ_0 increases, the G also increases.

When the chip is peeling, the peeling force P_f is affected by the geometric relationship between the peeling angle θ_p and the bending deflection of the chip. As shown in Figure 3b, let b be the adhesive width, and the relationship is as follows:

$$\begin{cases} F_L = E_{film}db \left(\frac{1}{\cos \theta_t} - 1 \right) \\ \theta_t = \theta_{B1} + \theta_p = \frac{3 \sin \theta_t F_L a^2}{2E_{chip}b\delta_{chip}^3} + \theta_p \end{cases} \quad (3)$$

From Equations (1) and (3), it can be seen that the peeling energy release rate G in the process of chip peeling is only related to the peeling angle θ_p and the geometric relationship, and the relationship is as follows:

$$G = \frac{1}{2}E_{film}d \left(\frac{1}{\cos \theta_t} - 1 \right)^2 + E_{film}d \left(\frac{1}{\cos \theta_t} - 1 \right) (1 - \cos \theta_p) \quad (4)$$

Therefore, it can be concluded that the peeling energy release rate G is primarily dependent on the peeling angle θ_p and the geometry during crack initiation. The peeling angle θ_p can therefore serve as an important parameter of the peeling energy release rate during the interface separation process. In addition, the peeling angle θ_p is easy to observe and measure during the peeling process, making it a key parameter in the analysis of chip peeling.

2.4. Mechanical Analysis of Crack Initiation Process

If the chip is thicker and more rigid, the deformation during peeling is small. As shown in Figure 8, the relationship between the peeling angle and the length of the chip and the fixed support boundary is as follows:

$$\tan \theta_p = \tan \theta_t = \frac{2h}{a_1 - a} \quad (5)$$

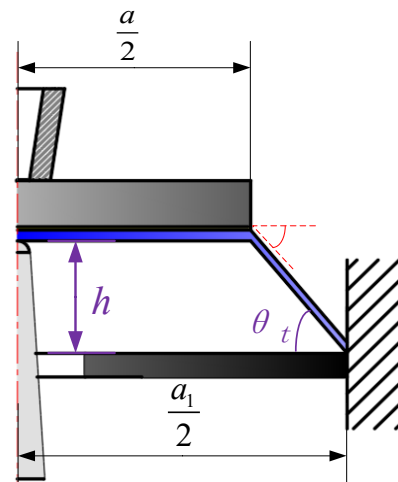


Figure 8. Diagram of the relationship between stripping Angle and chip and fixed support boundary size.

When the chip becomes larger and thinner, the flexibility becomes stronger, and the deformation is larger during peeling. As shown in Figure 9, the actual peeling angle θ_p is computed as the difference between the deflection angle θ_t of the soft film and the maximum rotation angle θ_B of the chip:

$$\theta_p = \theta_t - \theta_B \approx \arctan\left(\frac{2(h - w_{B1})}{a_1 - a}\right) \quad (6)$$

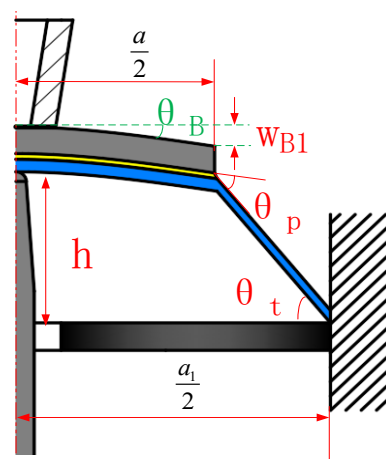


Figure 9. Mechanical model of crack initiation.

A comparison between the two indicates that the peel angle decreases as the bending deflection of the chip increases. This occurs because the film tension is harder to convert into an effective peel force, leading to a decreased energy release rate during peeling and a reduced likelihood of interface crack initiation.

Furthermore, Kovalchick has discovered that the crack initiation and propagation are also related to the peeling rate. The energy G_E required for peeling varies with the interface peeling rate v_c , and the two show a power-law relationship as shown in Equation (7):

$$G_E(v) = G_0 \left(\frac{v}{v_0} \right)^\varepsilon \quad (7)$$

where v_0 is the peeling rate, G_0 is the energy required for peeling, v is the actual peeling rate, and ε is a power-law constant (determined by the properties of the chip and the adhesive material).

The adhesion peeling initial crack is shown in Figure 10. The length of the cohesive zone is Δc and the length is about 10 μm . If the peeling angle remains approximately unchanged during the crack initiation, the relationship between needle speed v_{needle} and the interface peeling rate v_c approximately satisfies Equation (8).

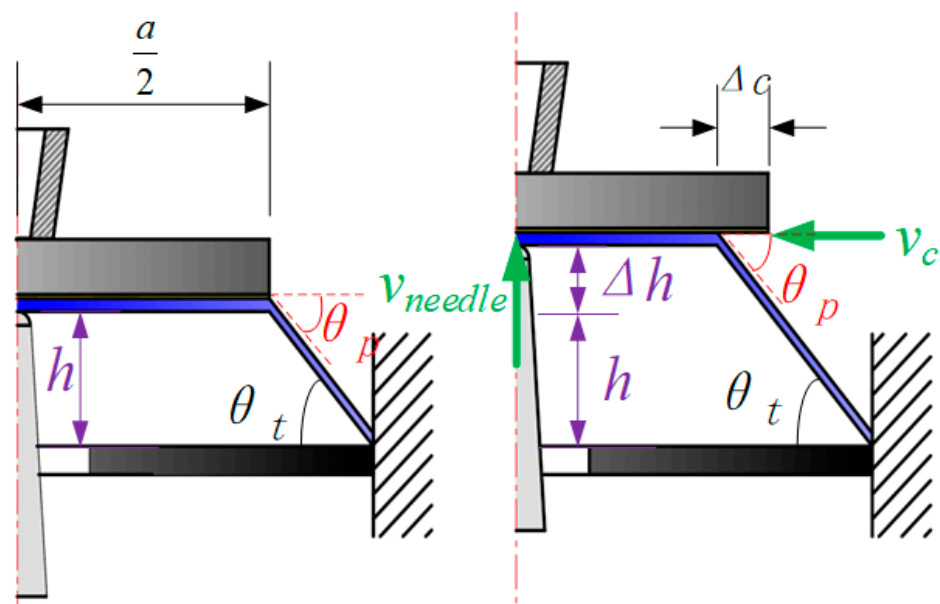


Figure 10. The process of crack initiation at the rigid die bond-peel interface during peeling.

$$v_c = \frac{v_{needle}}{\tan \theta_p} = \frac{v_{needle}}{\tan \theta_t} \quad (8)$$

Equation (8) shows that the required peeling energy is positively related to the needle lifting rate, which is deduced as Equation (9).

$$G_c = G_E(v) \propto v_c^n = G_E(v) \propto v_{needle}^n \quad (9)$$

where n is a constant related to base film material, substrate material, size specification, type of adhesive, etc.

When the chip becomes larger and thinner, its flexibility increases. If the needle exerts force as shown in Figure 11, the bending deformation of the chip increases, thus compressing the peeling angle θ_p in the mechanical model to θ_{p1} . Consequently, the interface peeling rate compared to the case of a rigid chip v_c is raised to v_{c1} , satisfying Equation (10).

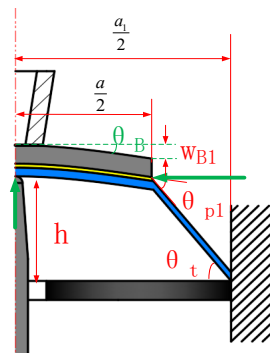


Figure 11. Initial crack initiation at the bond–peel interface of flexible chips during peeling.

$$v_{c1} = \frac{v_{needle}}{\tan \theta_{p1}} = \frac{v_{needle}}{\tan(\theta_{t1} - \theta_B)} > v_c \quad (10)$$

Equation (10) shows that the required peel energy is increased compared to rigid chips, which is expressed as:

$$G_c = G_E(v) \propto v_{c1}^n > G_E(v) \propto v_c^n \quad (11)$$

To enhance the peeling performance, the pushing velocity v_{needle} is continuously increased. This leads to an increase in the interface peeling energy G_c that needs to be overcome, necessitating a higher energy release rate for successful peeling. Consequently, crack initiation becomes challenging.

3. Results and Discussion

As discussed earlier, the size, thickness, and peeling speed of the chip all impact the initial interface crack generation process. These effects can be correlated and characterized by the peeling angle to a certain extent. In order to better understand this relationship, a three-dimensional finite element model of the peeling system was constructed in combination with the CZM unit to simulate the peeling process.

The chip, collector, and needle materials are shown in Table 2. In the chip peeling experiment, the thickness of the adhesive layer was only 5 μm , which is much smaller than the thickness of the blue film and the chip. It was no longer set separately in the geometric model and was replaced by the cohesive zone unit embedded in the zero-thickness layer by the finite element calculation platform.

Table 2. Simulation parameter settings.

	Materials	Elastic Modulus	Poisson's Ratio
Chip	Silicon substrate	129 GPa	0.28
Blue film	PVC	148 MPa	0.3
Needle	Structural steel	200 GPa	0.3
Collector	Structural steel	200 GPa	0.3

The downward pressure of the collector was 0.08 N, and the peeling process was simulated over a time of 1×10^{-4} s. The tip radius of the needle was 0.025 mm. The thickness of the blue film was 0.075 mm, and the width of the chip was 0.2 mm.

3.1. Influence of Chip Size on Crack Initiation

We set the chip thickness to $\delta = 0.03$ mm and the needle pushing speed $v_{needle} = 0.2$ mm/5 ms. Two cases of $a = 0.4$ mm, $a_1 = 1.2$ mm and $a = 2$ mm, $a_1 = 2.8$ mm were selected for the simulation, and the influence of the chip size on crack initiation was analyzed.

The change process of peeling angle and peeling force in the two cases is shown in Figure 12. When $a = 0.4$ mm, the chip did not bend significantly during the whole crack initiation process, and the peeling angle was approximately equal to the deflection angle of the blue film. The initial crack was produced at a lifting height of 0.0993 mm, with the peeling angle and peeling force reaching 12.54788° and 0.02325 N, respectively. In contrast, when $a = 2$ mm, the crack did not initiate even when the lifting height was 0.2 mm, and the peeling angle and peeling force were considerably smaller than the former. This indicates that as the chip size increases, its deformation increases, leading to a smaller peeling angle at the same lifting height, and a more difficult crack initiation. These results align with the analytical findings.

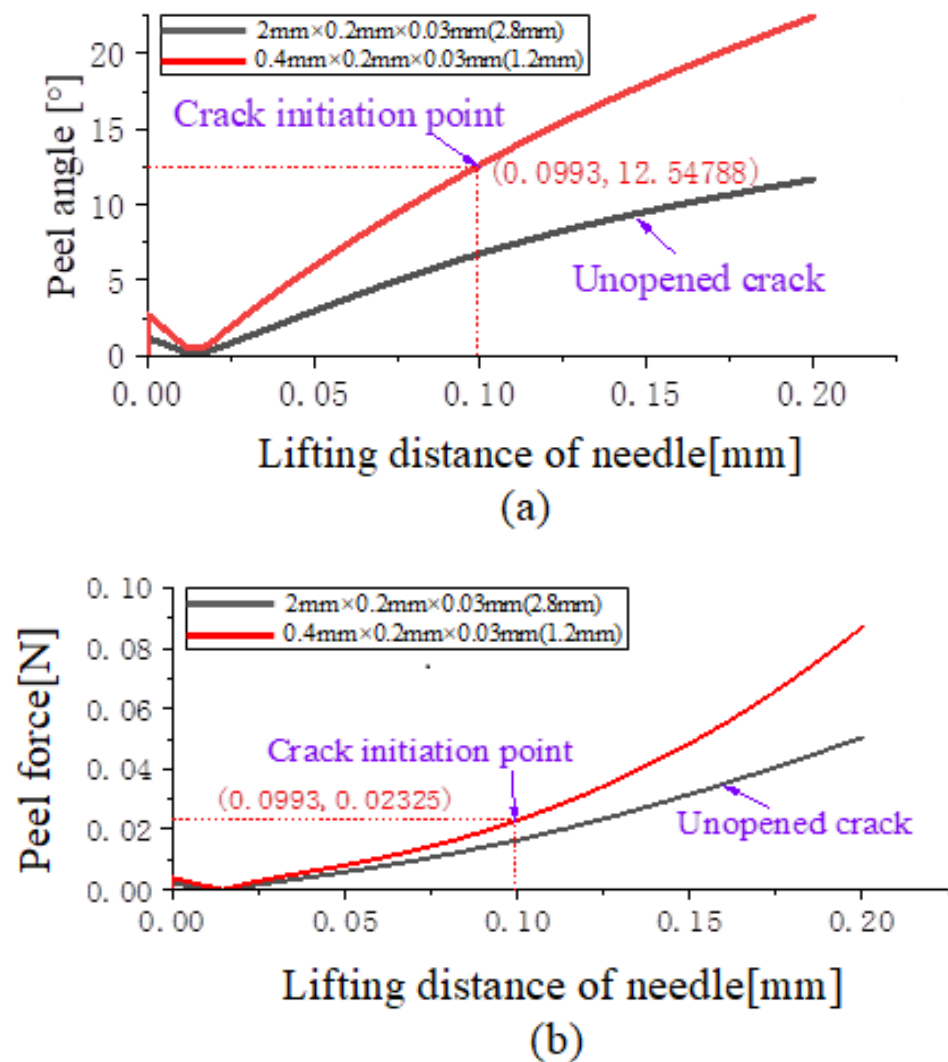


Figure 12. Comparison of changing chip length when $v_{\text{needle}} = 0.2$ mm/5 ms. (a) Peeling angle change curve; (b) Peel force change curve.

3.2. Influence of Chip Thickness on Crack Initiation

We set $a = 2$ mm, $a_1 = 2.8$ mm, needle lifting speed $v_{\text{needle}} = 0.2$ mm/5 ms, and chip thickness $\delta = 0.03$ mm or $\delta = 0.1$ mm. The influence of the chip thickness on crack initiation is analyzed.

The changes in peeling angle and peeling force were analyzed in two cases, as shown in Figure 13. In the first case, when $\delta = 0.1$ mm, the crack initiation was completed when the chip was lifted to 0.1815 mm, and the peeling angle and peeling force reached 16.60008° and 0.03493 N, respectively. In the second case, when $\delta = 0.03$ mm, the crack was not

initiated even if the chip was lifted to 0.2 mm; the peeling angle was only 11.6672° and the peeling force reached 0.05047 N.

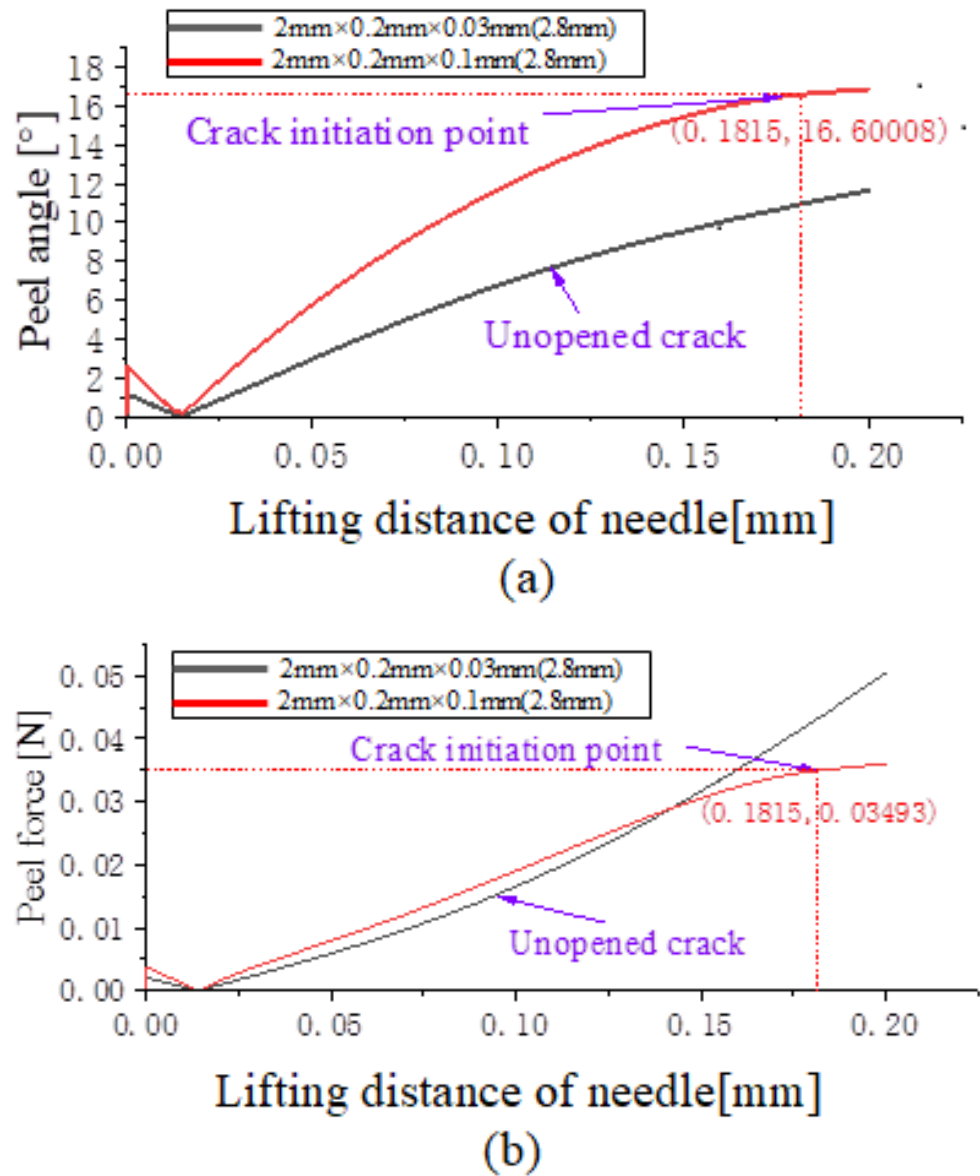


Figure 13. Comparison of changing chip thickness when $v_{\text{needle}} = 0.2 \text{ mm}/5 \text{ ms}$. (a) Peeling angle change curve; (b) Peel force change curve.

3.3. Influence of Lifting Speed on Crack Initiation

We set $\delta = 0.03 \text{ mm}$, and $a = 0.4 \text{ mm}$, $a_1 = 1.2 \text{ mm}$ or $a = 2 \text{ mm}$, $a_1 = 2.8 \text{ mm}$. In both cases, the needle lift speed was set to $v_{\text{needle}} = 0.2 \text{ mm}/5 \text{ ms}$ and $v_{\text{needle}} = 0.2 \text{ mm}/500 \text{ ms}$, and influence of lifting speed on crack initiation was analyzed.

The comparison of the peeling angle and peeling force in the two cases is shown in Figure 14. Both cases achieved initial crack germination at a lift of 0.0993 mm. The peeling angle and peeling force at 5 ms and 500 ms were 12.54788° and 0.02325 N and 12.53796° and 0.02266 N, respectively; the former increased by about 0.079% and 2.6%, indicating that the increase in the lifting rate leads to an increase in the energy required for initial peeling, which is consistent with the analytical results.

The comparison between the peeling angle and peeling force in the two cases is shown in Figure 15. The data results are consistent and indicate that the traditional peeling method is unable to initiate the crack, even if the lifting time is slowed down to an unacceptable

level of 5 ms to 500 ms. This highlights the difficulty of crack initiation through traditional peeling techniques.

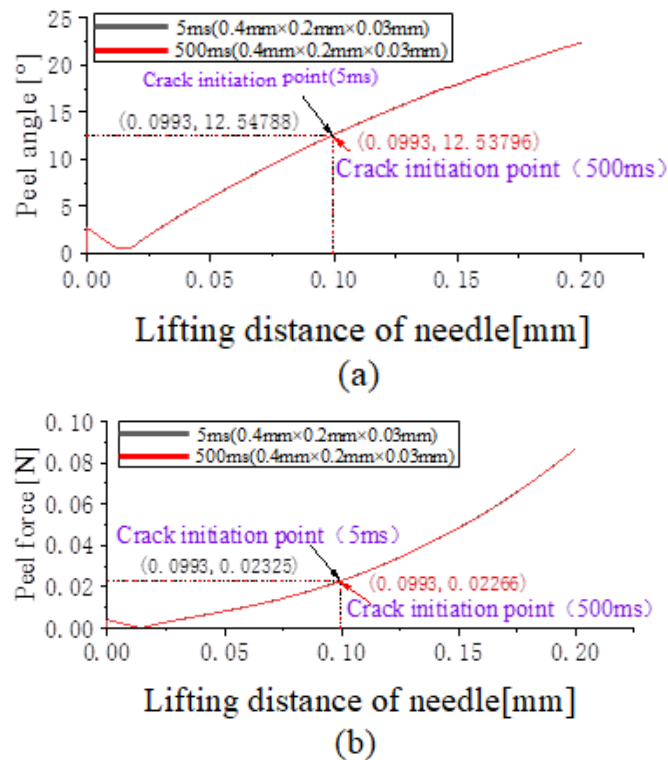


Figure 14. Comparison of changing lifting rate when $a = 0.4\text{ mm}$, $a_1 = 1.2\text{ mm}$, $\delta = 0.03\text{ mm}$. (a) Peeling angle change curve; (b) peel force change curve.

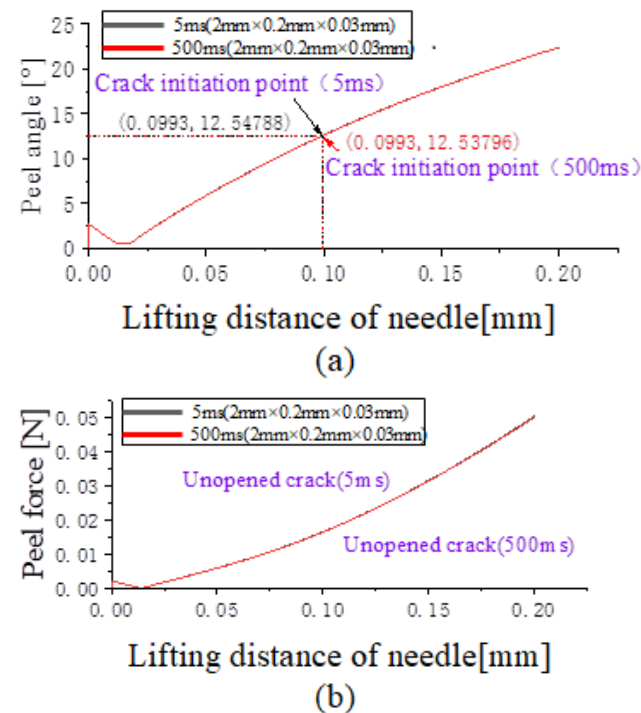


Figure 15. Comparison of changing lifting rate when $a = 2\text{ mm}$, $a_1 = 2.8\text{ mm}$, $\delta = 0.03\text{ mm}$. (a) Peeling angle change curve; (b) peel force change curve.

3.4. Stress of Chip during Crack Initiation

We set the lifting velocity $v_{needle} = 0.2 \text{ mm/5 ms}$, $\delta = 0.03 \text{ mm}$, $a = 0.4 \text{ mm}$, $a_1 = 1.2 \text{ mm}$, $\delta = 0.03 \text{ mm}$ or $a = 2 \text{ mm}$, $a_1 = 2.8 \text{ mm}$, $\delta = 0.1 \text{ mm}$, or $a = 2 \text{ mm}$, $a_1 = 2.8 \text{ mm}$. The changes in chip stress during the crack initiation under the three conditions are shown in Figure 16. In the first two cases, the chip stress remained within safe levels (the limit value of 1% probability fracture damage strength of silicon substrate, which is about 71 MPa when $\delta = 100 \text{ }\mu\text{m}$ and about 345 MPa when $\delta = 30 \text{ }\mu\text{m}$), indicating that this peeling method is effective for chips with a smaller size or larger thickness, and can meet the requirements of crack initiation. However, in the third case, the chip stress exceeded the safety limit before the crack was initiated during the lifting process, resulting in damage or even fracture. Even when $a = 2 \text{ mm}$, $a_1 = 2.8 \text{ mm}$, $\delta = 0.03 \text{ mm}$, and the lifting velocity was reduced to 1%, the initial crack still could not be initiated. This suggests that as the chip becomes larger and thinner, reducing the lifting rate is not a feasible way to achieve crack initiation with the traditional peeling method.

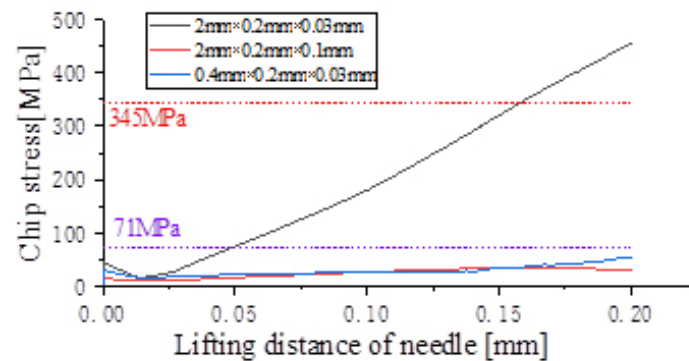


Figure 16. The maximum equivalent stress change curve of the chip ($v_{needle} = 0.2 \text{ mm/5 ms}$).

The influence of lifting velocity on the maximum equivalent stress of the chip is shown in Figure 17. When $a = 2 \text{ mm}$, $a_1 = 2.8 \text{ mm}$, and $\delta = 0.03 \text{ mm}$, compared $v_{needle} = 0.2 \text{ mm/500 ms}$ with $v_{needle} = 0.2 \text{ mm/5 ms}$, the ultimate stress of the chip was reduced from 455.17 MPa to 451.32 MPa, indicating a reduction of about 8.46%. If $a = 0.4 \text{ mm}$, $a_1 = 1.2 \text{ mm}$, and $\delta = 0.03 \text{ mm}$, the peeling process became easier with a slower lifting velocity, but it only changed the equivalent maximum stress of the chip from 53.043 MPa to 53.215 MPa, showing a difference of only 3.24%. Even if the lifting rate was reduced by 100 times, the variation range of the equivalent maximum stress of the chip was different by a few thousandths of a MPa. This indicates that the effect of reducing the lifting velocity on reducing the equivalent maximum stress of the chip is not obvious.

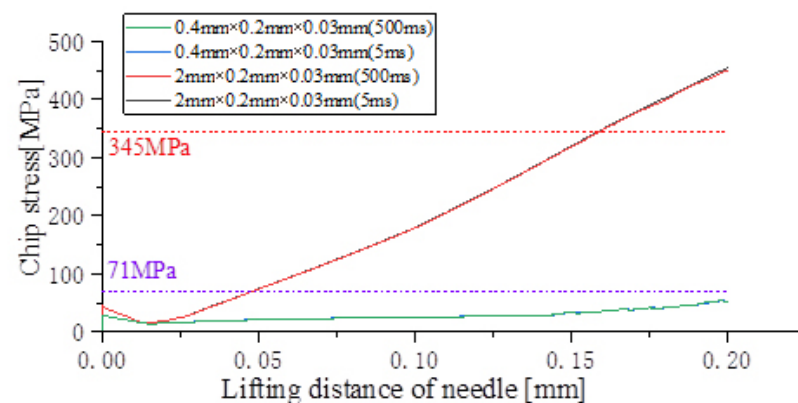


Figure 17. Change curve of chip maximum equivalent stress under changing jacking rate ($v_{needle} = 0.2 \text{ mm/5 ms}$ and $v_{needle} = 0.2 \text{ mm/500 ms}$).

4. Coupled Initiation Mode of Adhesive Interfacial Crack

4.1. Principle of Coupling Initiation

The analysis above shows that with the increase of chip size and thickness, the probability of chip damage and fragmentation increases, and the initial stripping becomes more and more difficult. Additionally, the importance of the peel angle in crack initiation and the way in which the geometric structure influences the peel angle suggest that structural optimization may offer a new solution for increasing the peel angle during crack excitation. Therefore, the peeling strategy including two features, structural coupling and force surface coupling, was proposed and is shown in Figure 18.

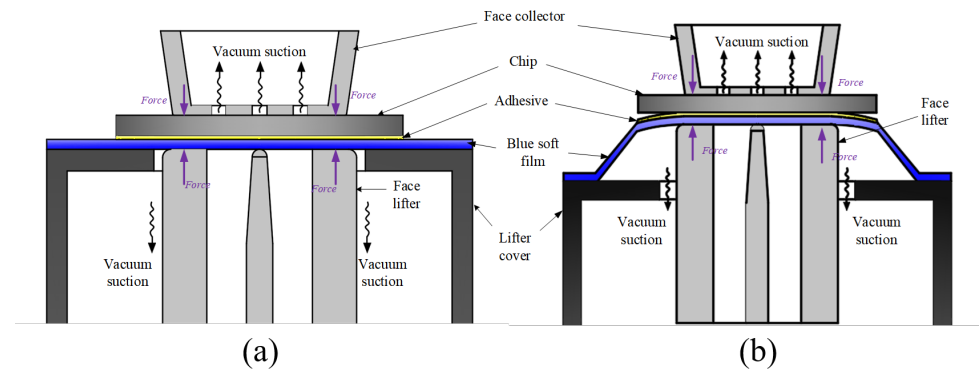


Figure 18. Schematic diagram of the crack coupling initiation strategy. (a) Initial state of face collector down pressure and face lifter coupling; (b) Initial state of face collector down pressure and face lifter coupling.

Firstly, the needle was redesigned as a face lifter embedded with the needle, and the displacement load is applied by the surface load (Figure 18a).

Secondly, the single hole suction nozzle (collector) was redesigned into a face collector with multi holes. At the beginning of peeling, the suction nozzle and the lifter surface are coupled with each other, and the coupling force surface is constructed by “lower pushing—upper pressing” to suppress the bending deformation of the chip during the crack initiation. Through structural coupling, the bending deformation of the chip is reduced, the change of peeling angle is controllable, and the effective peeling force is improved. Through force surface coupling, chip local stiffness is also improved, leading to a reduction in deformation and stress.

After the completion of the interface crack initiation, the interface crack propagation process begins. The phased control strategy process for crack propagation is shown in Figure 19.

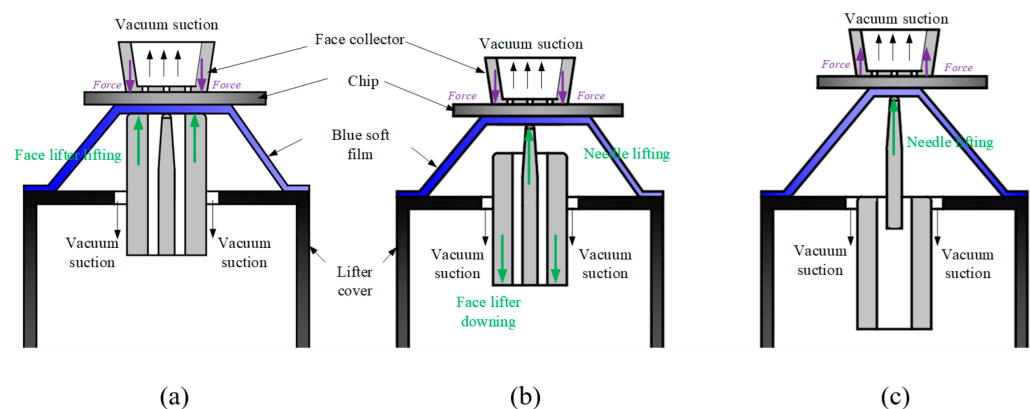


Figure 19. Staged control strategy for crack propagation. (a) Face-lifter lifting crack propagation stage; (b) needle lifting crack propagation stage; (c) crack propagation end stage.

- (1) After the completion of the coupled strategy for interface crack initiation, the lifting surface continues to lift, and the crack begins to propagate. The contact area between the chip and the blue film interface gradually decreases until the blue film, which has completed the expansion, is about to contact the lifted structure of the surface. The crack propagation will be hindered by the lifted structure of the surface.
- (2) Due to the fact that the lifting surface will hinder the propagation of the crack, the top needle is chosen to replace the lifting surface to continue lifting, in order to avoid the situation where the lifting surface affects the peel angle and interferes with the initiation of the peel energy release rate, which ultimately leads to a slowdown of the crack propagation rate. Therefore, it is necessary to control the rapid descent of the lifting surface.
- (3) The top needle continues to lift until the crack propagates to around 70–80% of the original interface contact area, and the crack propagation is completed. Finally, only the swing arm is needed to control the suction cup to lift and continue to operate to complete the transfer of the chip.

Under the coupling action of the structure and force plane, only the part of the chip outside the coupling area is involved in the peeling, which reduces the length of the chip involved in the peeling and reduces the length thickness ratio of the chip. In fact, the step-difference needle implemented by Swiss Bessie, the gas needle proposed by Jeon of Korea, and the multi-thimble needle presented by Peng and Yin of Huazhong University of Science and Technology all imply the idea of structural coupling excitation. In essence, they are all specific applications of this strategy.

4.2. Optimization of Mechanical Properties

By comparing the mechanical characteristics before and after the coupling method, the optimization effect was analyzed. The simplified model of the chip in the traditional mode is shown in Figure 20, and the maximum deflection W_{B1} of the bending part is:

$$W_{B1} = \frac{F_L \sin \theta_t \left(\frac{a}{2}\right)^3}{3E_{chip} I_{chip}} = \frac{F_L \sin \theta_t}{2E_{chip} b} \left(\frac{a}{\delta}\right)^3 \quad (12)$$

The maximum rotation angle θ_{B1} is:

$$\theta_{B1} = \frac{3F_L \sin \theta_t (a)^2}{2E_{chip} b \delta^3} = \frac{3F_L \sin \theta_t}{2E_{chip} b \delta} \left(\frac{a}{\delta}\right)^2 \quad (13)$$

The maximum stress σ'_{max} of the chip is:

$$\sigma'_{max} = \frac{3F_L \sin \theta_t (a)}{b \delta^2} \frac{F_L \cos \theta_t}{b \delta} \quad (14)$$

The peeling angle θ_p is:

$$\theta_p = \arctan \left(\frac{2(h - W_{B1})}{a_1 - a} \right) - \theta_{B1} \quad (15)$$

The mechanical model under the coupling mode is shown in Figure 21. The deformation area of the chip is limited to the part between the edge of the coupling surface and the edge of the chip, and the chip bends with the edge of the coupling surface as the origin and is symmetrical on the left and right.

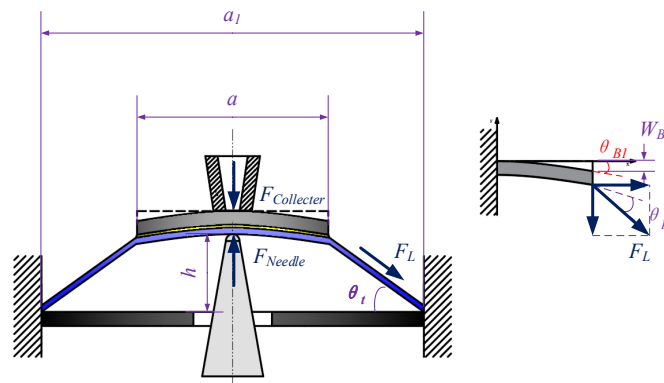


Figure 20. Simplified model of chip peeling and adhesion using traditional strategy.

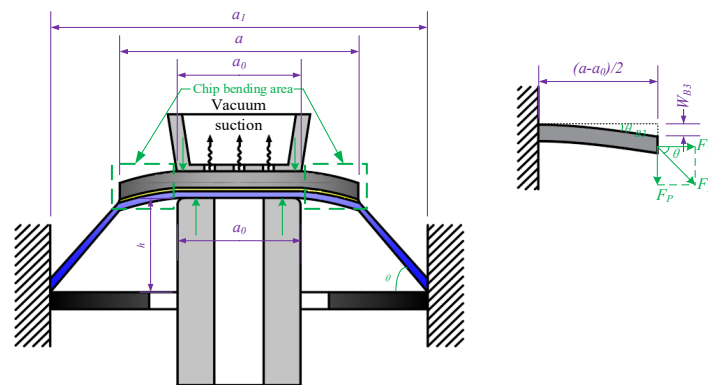


Figure 21. Simplified model of chip peel-off adhesion using coupling strategy.

The maximum deflection W_{B3} of the bending part is:

$$W_{B3} = \frac{F_L \sin \theta_t \left(\frac{a-a_0}{2}\right)^3}{3E_{chip} I_{chip}} = \frac{F_L \sin \theta_t}{2E_{chip} b} \left(\frac{a-a_0}{\delta}\right)^3 \quad (16)$$

The maximum rotation angle θ_{B3} is:

$$\theta_{B3} = \frac{3F_L \sin \theta_t (a-a_0)^2}{2E_{chip} b \delta^3} = \frac{3F_L \sin \theta_t}{2E_{chip} b \delta} \left(\frac{a-a_0}{\delta}\right)^2 \quad (17)$$

The maximum stress σ_{max} of the chip is:

$$\sigma_{max} = \frac{3F_L \sin \theta_t (a-a_0)}{b \delta^2} \frac{F_L \cos \theta_t}{b \delta} \quad (18)$$

The peeling angle θ'_p is:

$$\theta'_p = \arctan\left(\frac{2(h - W_{B3})}{a_1 - a}\right) - \theta_{B3} \quad (19)$$

Under the action of the coupling force, the effective length thickness ratio involved in the peeling process changes from a/δ_{chip} to $(a_1 - a)/\delta_{chip}$, and the length thickness ratio of the chip involved in crack initiation decreases. With this change, the length thickness ratio of the chip involved in crack initiation decreases and the peeling angle θ_p ($\theta_p = \theta_t - \theta_B$) is much larger compared to the traditional mode. The essence of the coupling action is to

transform the peeling of large-scale ultra-thin chips into a small-size thick chip peeling. The size design of the coupling force surface should satisfy the following relationship:

$$\sigma_{\max} = \frac{3F_L \sin \theta_t (a - a_0)}{b\delta^2} + \frac{F_L \cos \theta_t}{b\delta} \leq [\sigma] \quad (20)$$

where $[\sigma]$ is the damage limit stress of the chip, and the size a_0 of the coupling surface should meet the following requirements:

$$a > a_0 \geq a - \frac{b\delta^2}{3F_L \sin \theta_t} [\sigma] + \frac{\delta}{3 \tan \theta_t} \quad (21)$$

5. Simulation Analysis on Crack Initiation Characteristics

As mentioned earlier, the face lifter is a surface structure with a needle embedded in the middle. Similarly, the face collector also has a surface structure. In theory, their surfaces can have different shapes. For simplicity, it is assumed that they have the same surface shape. Crack initiation characteristics can be analyzed with simulations. The basic parameters of the geometry and materials are shown in Table 3.

Table 3. Simulation parameter settings.

	Materials	Elastic Modulus	Poisson's Ratio
Chip	Silicon substrate	129 GPa	0.28
Blue film	PVC	148 MPa	0.3
Face lifter	Structural steel	200 GPa	0.3
Face collector	Structural steel	200 GPa	0.3

The chip specifications of the simulation model were $a = 2$ mm, $a_1 = 2.8$ mm, and $\delta = 0.03$ mm. The thickness of the coupling structure (simplified face lifter and collector) was 0.05 mm and the width was 0.18 mm. In the crack initiation, the surface suction nozzle was contacted and pressed down (the time required for the down pressure to be 0.08 N was set to 1×10^{-4} s), and then the face lifter was pushed up.

5.1. Peeling Angle and Chip Stress in Coupling Mode

The lifting velocity was set to $v_{\text{Face}} = 0.2$ mm/5 ms, and the coupling size was $a_0 = 1.2$ mm. The comparative analysis between the coupling mode and the traditional mode is shown in Figure 22. In the coupling mode, the chip was successfully lifted up to 0.04444 mm, with a peeling angle of 6.42462° and a peeling force of 0.00986 N. In contrast, the traditional mode could not lift the chip at 5 ms/0.2 mm, and the crack could only be initiated at a higher speed. Additionally, the peeling angle in the coupling mode was significantly larger, and the peeling force was effectively improved in comparison to the traditional mode.

The chip stress in the coupling mode is shown in Figure 23; the maximum stress of the chip was 98.907 MPa, which is significantly lower than that in the traditional mode, which exceeded the safety limit of 345 MPa.

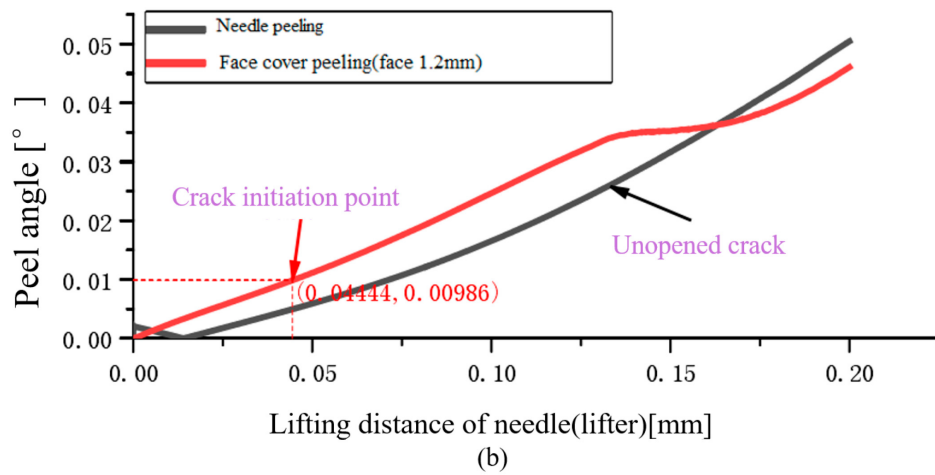
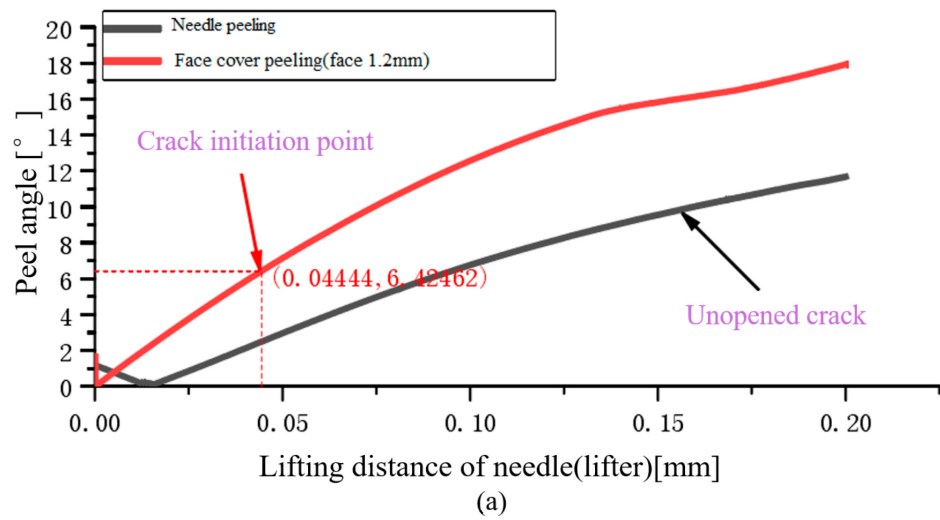


Figure 22. The coupling strategy is compared with the traditional method, when $a = 2$ mm, $a_1 = 2.8$ mm, $a_0 = 1.2$ mm, $\delta = 0.03$ mm ($v_{Face} = 0.2$ mm/5 ms) (a) Peeling angle change curve; (b) peel force change curve.

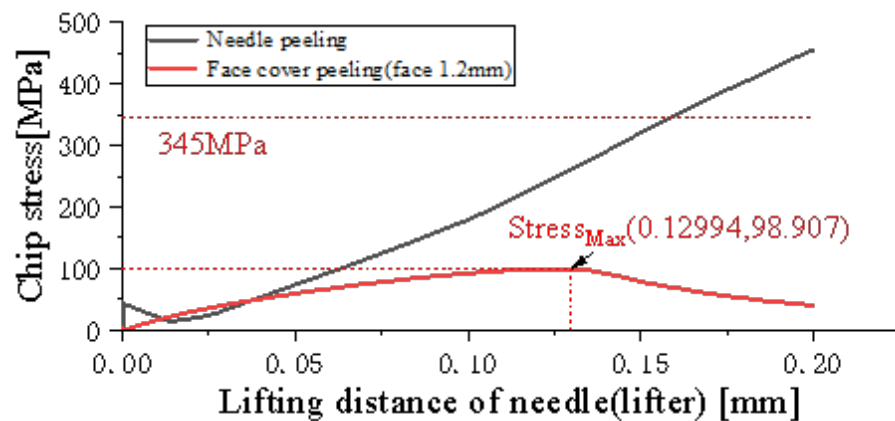


Figure 23. When $v_{Face} = 0.2$ mm/5 ms ($a_0 = 1.2$ mm), the difference in chip stress between coupling strategy and traditional method.

This shows that the coupling strategy can obviously reduce the chip stress during the crack initiation of large-size ultra-thin chip peeling. The safety and reliability have been greatly improved.

5.2. Influence of Lifting Velocity Size in Coupling Mode

We set $a_0 = 1.2$ mm, the lifting velocity as $v_{Face1} = 0.2$ mm/500 ms or $v_{Face2} = 0.2$ mm/5 ms, and analyzed influence of the lifting velocity.

The results are shown in Figure 24. When the lift time $t = 5$ ms, the crack was initiated when it was lifted to 0.04444 mm; the peeling angle and peeling force were 6.27859° and 0.0095 N, respectively. When $t = 500$ ms, the crack was initiated when it was lifted to 0.04344 mm; the peeling angle and peeling force were 6.42462° and 0.00986 N, respectively. With an increase in lifting distance by 0.001 mm, the corresponding peeling angle and peeling force increased by 2.33% and 3.79%. The results indicate that under the coupling strategy, secure crack initiation can be achieved without reducing the lifting velocity. This finding is consistent with the conclusion of the aforementioned analysis.

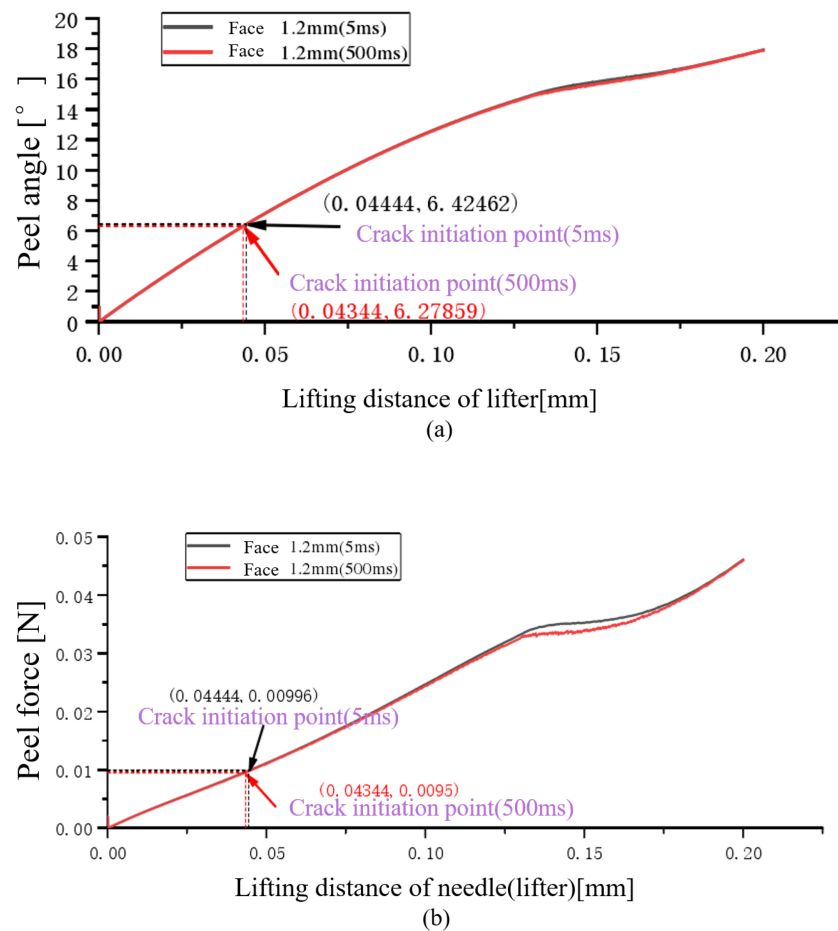


Figure 24. Under the coupling strategy, the comparison of changing the jacking rate when $a = 0.4$ mm, $a_1 = 1.2$ mm, $\delta = 0.03$ mm. (a) Peeling angle change curve; (b) peel force change curve.

5.3. Influence of Coupling Surface Size in Coupling Mode

We set $v_{Face} = 0.2$ mm/5 ms, and the size of the coupling surface is set to $a_0 = 0.6$ mm or $a_0 = 1.2$ mm for comparative analysis.

The results are presented in Figure 25, where it can be observed that the 0.6 mm chip initiated a crack when lifted to 0.05169 mm, while in Figure 26, the 1.2 mm chip initiated a crack when lifted to 0.04444 mm. The peeling angle of the 1.2 mm chip was larger than that of the 0.6 mm chip, with the peeling angle and peeling force of the 0.6 mm chip being 5.631° and 0.01026 N, respectively, whereas those of the 1.2 mm chip were 6.42462° and 0.00986 N, respectively.

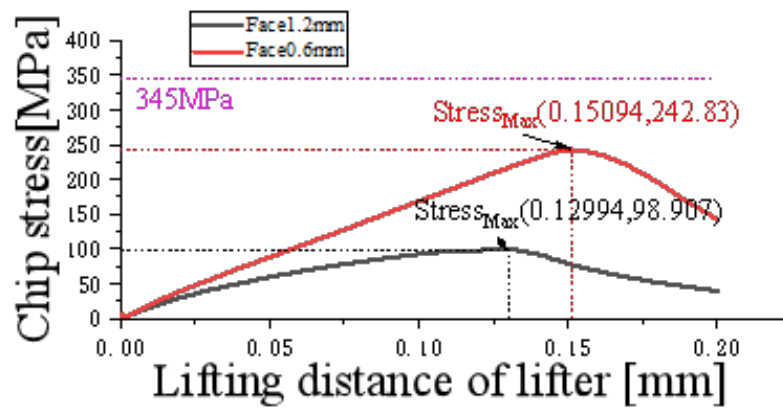


Figure 25. Under the coupling strategy, when $v_{Face} = 0.2 \text{ mm/5 ms}$, the change in the chip stress with changing size of the coupling surface.

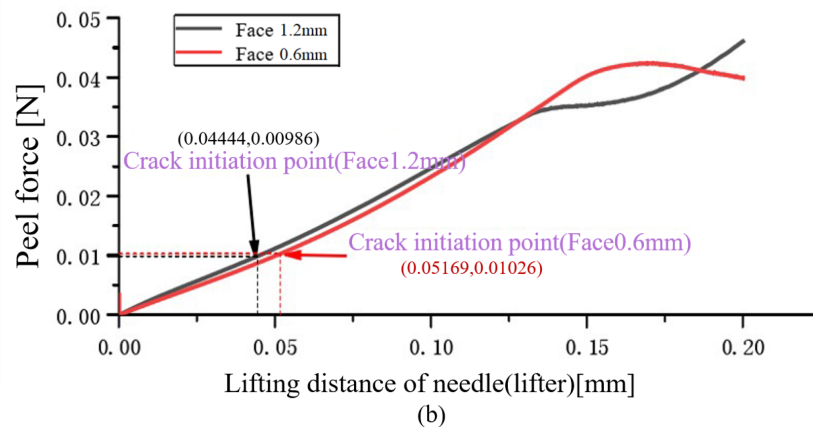
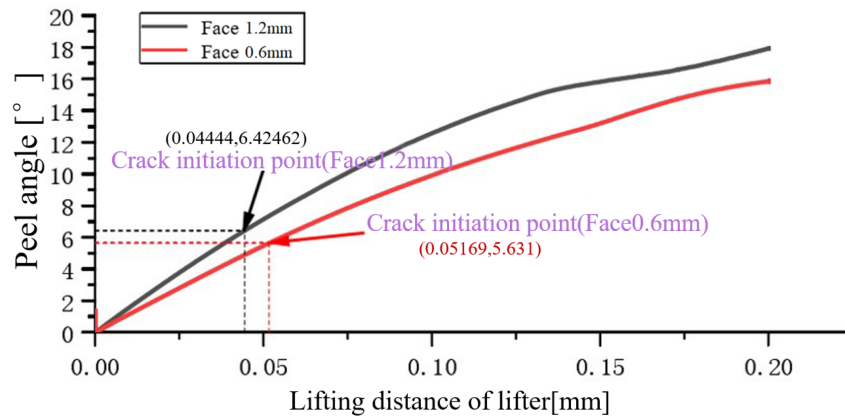


Figure 26. Under the coupling strategy, the comparison of changing the coupling surface size when $a = 2 \text{ mm}$, $a_1 = 2.8 \text{ mm}$, $\delta = 0.03 \text{ mm}$ ($v_{needle} = 0.2 \text{ mm/5 ms}$). (a) Peeling angle change curve; (b) peel force change curve.

In addition, when $a_0 = 0.6 \text{ mm}$, the chip stress during the lifting process was greatly increased compared with that when $a_0 = 1.2 \text{ mm}$. As shown in Figure 26, the maximum stress was increased to 242.83 MPa, an increase of 145.51%, indicating that the chip stress has an important relationship with the coupling structure; thus, the design of the coupling size is very important for the safe stripping of the initial interface.

The coupling strategy improves the stiffness of the chip in the coupling area, and the chip transforms from the overall large deflection deformation to the local small deflection

deformation, which essentially linearizes the nonlinear deformation problem of the large-scale ultra-thin chip and realizes controllable crack initiation. This strategy improves the peeling angle conditions in the crack initiation process, enabling effective conversion of blue film tensile force into peeling force and reducing the local stress of the chip. Consequently, even at higher peeling velocities, the crack can be safely initiated.

6. Conclusions

This paper presents an adhesive peeling model based on the cohesive zone model to analyze the fast and non-destructive peeling characteristics of large-size ultra-thin chips. The results show that large deflection deformation leads to a decrease in the peeling angle, resulting in difficulties in improving the peeling force and energy release rate. To address this, a coupling peeling strategy was proposed to increase the peeling angle during crack germination. This strategy employs structural coupling to improve the local flexibility of the chip and utilizes force surface coupling to improve the overall stiffness of the chip, especially a part of the coupling area, thereby improving the control conditions of the peeling angle. Mechanical analysis and 3D simulation based on a CZM unit showed that, compared with the traditional peeling process, the coupling strategy increased the strain mismatch effect between the chip and the soft membrane promoting rapid peeling angle excitation and increasing the peeling energy release rate. Additionally, the surge of chip stress can be effectively restrained, thereby improving the peeling safety and reliability.

The coupling strategy improved the stiffness of the chip in the coupling area, so that the chip peeling transforms from the overall large deflection deformation to a local small deflection deformation. This strategy improves the peel angle control conditions in the crack initiation process, promotes the effective conversion of the blue film tensile force into the peel force, reduces the local stress of the chip, can be safely initiated even at a higher peel rate, and improves the peeling performance. However, after the crack successfully initiates, it will rapidly expand. If handled improperly, the coupling structure will form obstacles. The following research will mainly focus on the coupled acceleration control of crack propagation in large-sized and ultra-thin chips, studying the mechanical characteristics of crack propagation acceleration, the coupled acceleration control strategy of crack propagation, selecting appropriate peeling methods, establishing a three-dimensional model, and conducting corresponding finite element analysis to determine the effect of coupled acceleration control on the variation in peeling angle.

Author Contributions: Conceptualization, T.W. and X.C.; methodology, X.C.; software, X.C.; validation, X.C., S.W. and F.L.; formal analysis, T.W.; investigation, X.C.; resources, T.W.; data curation, S.W.; writing—original draft preparation, X.C.; writing—review and editing, T.W.; visualization, F.L.; supervision, T.W. and S.L.; project administration, T.W. and X.C.; funding acquisition, T.W. and S.L. All authors have read and agreed to the published version of the manuscript.

Funding: This research was supported by the Guangdong Natural Science Foundation Project, China (No. 2021A1515010661), and the Guangdong province Science and Technology Plan Project (grant No. STKJ2021027).

Institutional Review Board Statement: Not applicable.

Informed Consent Statement: Not applicable.

Data Availability Statement: Not applicable.

Conflicts of Interest: The authors declare no conflict of interest.

References

1. Liu, X.; Li, M.; Zheng, J.; Zhang, X.; Zeng, J.; Liao, Y.; Chen, J.; Yang, J.; Zheng, X.; Hu, N. Electrochemical Detection of Ascorbic Acid in Finger-Actuated Microfluidic Chip. *Micromachines* **2022**, *13*, 1479. [[CrossRef](#)]
2. Craig, P.; Ng, R.; Tefsen, B.; Linsen, S.; Liu, Y.; Hendel, J. Information Visualisation for Antibiotic Detection Biochip Design and Testing. *Processes* **2022**, *10*, 2680. [[CrossRef](#)]

3. Ho, C.-H.; Chen, S.-M.; Wu, Y.-R. Study of the Factors Limiting the Efficiency of Vertical-Type Nitride- and AlInGaP-Based Quantum-Well Micro-LEDs. *Processes* **2022**, *10*, 489. [[CrossRef](#)]
4. Yeom, D.; Kim, J.; Kim, S.; Ahn, S.; Choi, J.; Kim, Y.; Koo, C. A Thermocycler Using a Chip Resistor Heater and a Glass Microchip for a Portable and Rapid Microchip-Based PCR Device. *Micromachines* **2022**, *13*, 339. [[CrossRef](#)]
5. Balamurugan, K.; Umamaheswaran, S.; Mamo, T.; Nagarajan, S.; Namamula, L.R. Roadmap for Machine Learning based Network-on-Chip (M/L NoC) technology and its analysis for researchers. *J. Phys. Commun.* **2022**, *6*, 022001. [[CrossRef](#)]
6. Christou, A.; Ma, S.H.; Zumeit, A.; Dahiya, A.S.; Dahiya, R. Printing of Nano- to Chip-Scale Structures for Flexible Hybrid Electronics. *Adv. Electron. Mater.* **2023**, *1*, 2201116. [[CrossRef](#)]
7. Behler, S.; Teng, W.; Podpod, A. Key Properties for Successful Ultra Thin Die Pickup. In Proceedings of the 2017 IEEE 67th Electronic Components and Technology Conference (ECTC), Orlando, FL, USA, 30 May–2 June 2017; pp. 95–101.
8. Yang, Y.; Wu, Y. Analysis of the Characteristics of UV Films and Blue Films Used in the Process of Chip Industrialization. *Mod. Electron. Technol.* **2013**, *36*, 3.
9. Canale, G.; Andrews, S.; Rubino, F.; Maligno, A.; Citarella, R.; Weaver, P.M. Realistic Stacking Sequence Optimisation of an Aero-Engine Fan Blade-Like Structure Subjected to Frequency, Deformation and Manufacturing Constraints. *Open Mech. Eng. J.* **2018**, *12*, 151–163. [[CrossRef](#)]
10. Zou, J.; Zhang, Y.; Zhang, L.; Jing, J.; Fu, Y.; Wang, Y.; Zhang, G.; Zhou, F. Numerical Simulation Research on the Effect of Artificial Barrier Properties on Fracture Height. *Processes* **2023**, *11*, 310. [[CrossRef](#)]
11. Neves, L.F.R.; Campilho, R.D.S.G.; Sánchez-Arce, I.J.; Madani, K.; Prakash, C. Numerical Modelling and Validation of Mixed-Mode Fracture Tests to Adhesive Joints Using J-Integral Concepts. *Processes* **2022**, *10*, 2730. [[CrossRef](#)]
12. Khan, S.A.; Rahimian Kolor, S.S.; King Jye, W.; Yidris, N.; Mohd Yusof, A.A.; Mohd Szali Januddi, M.A.F.; Tamin, M.N.; Johar, M. Strain Rate Effect on Mode I Debonding Characterization of Adhesively Bonded Aluminum Joints. *Processes* **2023**, *11*, 81. [[CrossRef](#)]
13. Hong, J.H.; Cheng, P.; Chen, W.; Guo, J.H.; Li, Y.L.; Liu, J.Z. Theoretical Modeling and Experimental Studies of Ultra-Thin Chip Transfer in Laser-Induced Forward Transfer. *IEEE Trans. Compon. Manuf. Technol.* **2022**, *12*, 570–577. [[CrossRef](#)]
14. Hong, J.H.; Chen, W.; Guo, J.H.; Cheng, P.; Li, Y.L.; Dong, W.T. Theoretical and experimental studies of spring-buffer chip peeling technology for electronics packaging. *Int. J. Fract.* **2022**, *236*, 109–124. [[CrossRef](#)]
15. Liu, Z.; Huang, Y.; Xiao, L.; Tang, P.; Yin, Z. Nonlinear characteristics in fracture strength test of ultrathin silicon die. *Semicond. Sci. Technol.* **2015**, *30*, 045005. [[CrossRef](#)]
16. Peng, B.; Huang, Y.; Yin, Z. Competing Fracture Modeling of Thin Chip Pick-Up Process. *IEEE Trans. Compon. Packag. Manuf. Technol.* **2012**, *2*, 1217–1225. [[CrossRef](#)]
17. Cheng, H.; Wu, J.; Yu, Q.; Kim-Lee, H.-J.; Carlson, A.; Turner, K.T.; Hwang, K.-C.; Huang, Y.; Rogers, J.A. An analytical model for shear-enhanced adhesiveless transfer printing. *Mech. Res. Commun.* **2012**, *43*, 46–49. [[CrossRef](#)]
18. Jeon, E.B.; Park, S.H.; Yoo, Y.S.; Kim, H.S. Analysis of Interfacial Peeling of an Ultrathin Silicon Wafer Chip in a Pick-Up Process Using an Air Blowing Method. *IEEE Trans. Compon. Packag. Manuf. Technol.* **2016**, *6*, 1696–1702. [[CrossRef](#)]
19. Williams, J.A.; Kauzlarich, J.J. The influence of peel angle on the mechanics of peeling flexible adherends with arbitrary load—Extension characteristics. *Tribol. Int.* **2005**, *38*, 951–958. [[CrossRef](#)]
20. Molinari, A.; Ravichandran, G. Stability of peeling for systems with rate independent decohesion energy. *Int. J. Solids Struct.* **2013**, *50*, 1974–1980. [[CrossRef](#)]
21. Molinari, A.; Ravichandran, G. Peeling of Elastic Tapes: Effects of Large Deformations, Pre-Straining, and of a Peel-Zone Model. *J. Adhes.* **2008**, *84*, 961–995. [[CrossRef](#)]
22. Kovalchick, C.; Molinari, A.; Ravichandran, G. An experimental investigation of the stability of peeling for adhesive tapes. *Mech. Mater.* **2013**, *66*, 69–78. [[CrossRef](#)]
23. Yin, H.B.; Liang, L.H.; Wei, Y.G.; Peng, Z.L.; Chen, S.H. Determination of the interface properties in an elastic film/substrate system. *Int. J. Solids Struct.* **2020**, *191–192*, 473–485. [[CrossRef](#)]
24. Zhang, L.; Wang, J. A generalized cohesive zone model of the peel test for pressure-sensitive adhesives. *Int. J. Adhes. Adhes.* **2009**, *29*, 217–224. [[CrossRef](#)]
25. Liu, Z. *Mechanism Study and Process Optimization of Non Destructive Peeling of Ultrathin Chips*; Huazhong University of Science and Technology: Wuhan, China, 2015.
26. Liu, D. *Research on Several Mechanical Problems of Multi field Coupled Laminated Structures*; Zhejiang University: Hangzhou, China, 2013.
27. Dai, W. *Analysis of Chip Stripping Process and Its Mechanism*; Huazhong University of Science and Technology: Wuhan, China, 2011.
28. Ni, J.; Wang, J. Research on the mechanism of thin chip fragmentation failure in IC cards. *Semicond. Technol.* **2004**, *04*, 40–44.
29. Shu, Z.; Peng, X.; Li, F.F.; Xu, Q. Cohesive zone model for prepreg tack based on probe test. *Acta Aeronaut. Astronaut. Sin.* **2018**, *39*, 280–292.

30. Kendall, K. Thin-film peeling-the elastic term. *J. Phys. D Appl. Phys.* **1975**, *8*, 1449–1452. [[CrossRef](#)]
31. Kendall, K. The adhesion and surface energy of elastic solids. *J. Phys. D Appl. Phys.* **1971**, *4*, 1186–1195. [[CrossRef](#)]

Disclaimer/Publisher’s Note: The statements, opinions and data contained in all publications are solely those of the individual author(s) and contributor(s) and not of MDPI and/or the editor(s). MDPI and/or the editor(s) disclaim responsibility for any injury to people or property resulting from any ideas, methods, instructions or products referred to in the content.